INSTITUTE OF PHYSICS PUBLISHING JOURNAL OF PHYSICS: CONDENSED MATTER

J. Phys.: Condens. Matter **13** (2001) 10593–10611 PII: S0953-8984(01)25635-5

Partial coherence effects on the imaging of small crystals using coherent x-ray diffraction

I A Vartanyants[1] **and I K Robinson**

Department of Physics, University of Illinois, 1110 West Green Street, Urbana, IL 61801, USA

Received 8 June 2001
Published 9 November 2001
Online at stacks.iop.org/JPhysCM/13/10593

Abstract

Recent achievements in experimental and computational methods have opened up the possibility of measuring and inverting the diffraction pattern from a single-crystalline particle on the nanometre scale. In this paper, a theoretical approach to the scattering of purely coherent and partially coherent x-ray radiation by such particles is discussed in detail. Test calculations based on the iterative algorithms proposed initially by Gerchberg and Saxton and generalized by Fienup are applied to reconstruct the shape of the scattering crystals. It is demonstrated that partially coherent radiation produces a small area of high intensity in the reconstructed image of the particle.

(Some figures in this article are in colour only in the electronic version)

1. Introduction

Even in the early years of x-ray studies [1–4] it was already understood that the diffraction pattern from small perfect crystals is directly connected with the shape of these crystals through Fourier transformation. Of course, in a real diffraction experiment on a 'powder' sample, where many particles with different shapes and orientations are illuminated by an incoherent beam, only an averaged shape of these particles can be obtained. For example, the simple Scherrer formula is the exact result for particles of spherical shape [3]. Until recently, it has not been possible to obtain the diffraction pattern from just *one* particle, let alone to invert the intensity data (with the loss of all phase information) into a real image of a particle shape.

New developments in experimental and computational methods have opened up the possibility of solving this problem. Current advances in experimental facilities (ESRF, APS, SPRING-8) provide high-energy, high-brightness x-ray beams with high degrees of coherence. The coherence lengths achievable with these synchrotron radiation sources are in the range of a few microns. Illuminating a particle of nanometre scale with such a highly coherent beam has allowed the observation of continuous interference diffraction patterns using modern 2D CCD detectors [5]. The diffraction from such nanocrystals is no longer comprised of sharp Bragg peaks, but is now a complicated intensity distribution centred at each reciprocal-lattice

[1] On leave from: Institute of Crystallography, RAS, Leninsky Prospekt 59, 117333 Moscow, Russia.

point. This continuous function can be measured on an arbitrarily fine scale in the vicinity of one of the Bragg peaks.

During the last few decades a number of efforts have been made to evolve theoretical and computational methods in optics and electron microscopy for inverting images from the scattered object to real space in the case where they are connected simply by the Fourier transform (FT). Various iterative procedures were proposed first by Gerchberg and Saxton [6] and then developed further by Fienup [7]. The basic idea of these methods is the following. Measured amplitudes and random phases are inverse Fourier transformed to obtain an initial estimate of the real-space structure of a complex-valued object. This is then updated by applying an appropriate real-space constraint and back-transformed. The type of constraint can vary depending on what supplementary information is available about an object. Typically, for a complex-valued object it is desirable to have real-space amplitude information [8, 9] and conversely, if we are seeking the amplitudes, its phases have to be known. This requirement also follows from the need to make a change in real space every cycle; otherwise the inverse FT simply reverses the forward FT. However, in some situations this information is not enough for obtaining a unique solution in reasonable computation time. As was shown in recent studies [10–12], an oversampling of diffraction data—more than twice the Nyquist frequency—was found to increase the convergence of this iteration procedure.

In most of the previous tests and applications of the iterative algorithms it was tacitly assumed that the incoming radiation is purely coherent. This assumption immediately led to a simple connection between the object shape and its scattered intensity via the FT. However, in a real experimental situation with modern synchrotron sources providing high degrees of coherence, this condition can be violated. In a number of recent papers, the influence of partial coherence of x-ray radiation on *diffraction* patterns was studied theoretically [13, 14] and experimentally [15]. The purpose of our study presented in this work is to investigate the effects of the partial coherence of the incoming radiation on the *reconstructed* image of the object.

The paper is organized as follows. Section 2 recalls the important aspects of the diffraction theory on small strained particles with coherent illumination. Section 3 gives a general formalism of scattering of partially coherent radiation by the same particles. Section 4 treats the influence of this partially coherent radiation on the reconstructed shape of small crystal objects.

2. Diffraction from a small particle with coherent illumination

It is well known (see for example [16, 17]) that the scattering amplitude $A(\boldsymbol{q})$ of coherent monochromatic radiation from an infinite crystal in the kinematical approximation is equal to

$$A(\boldsymbol{q}) = \int \rho(\boldsymbol{r}) \mathrm{e}^{-\mathrm{i}\boldsymbol{q}\cdot\boldsymbol{r}}\, \mathrm{d}\boldsymbol{r} \tag{1}$$

where $\rho(\boldsymbol{r})$ is an electron density at the point $\boldsymbol{r}$, $\boldsymbol{q} = \boldsymbol{k}_f - \boldsymbol{k}_i$ is the momentum transfer, $\boldsymbol{k}_i$ and $\boldsymbol{k}_f$ are the incident and scattered wave vectors ($|\boldsymbol{k}_i| = |\boldsymbol{k}_f| = 2\pi/\lambda$, λ is the wavelength), the notation $\boldsymbol{a}\cdot\boldsymbol{b}$ is used for a scalar product of two vectors $\boldsymbol{a}$ and $\boldsymbol{b}$ and the integration extends over the whole volume of the crystal. The electron density can be put in the form of a sum of terms corresponding to individual atoms:

$$\rho(\boldsymbol{r}) = \sum_{n=1}^{N}\sum_{j=1}^{S} \rho_{nj}(\boldsymbol{r} - \boldsymbol{R}_{nj} - \boldsymbol{u}(\boldsymbol{R}_{nj}))$$

where $\boldsymbol{R}_{nj} = \boldsymbol{R}_n + \boldsymbol{r}_j, \boldsymbol{R}_n$ is the position of the nth unit cell in a perfect lattice, $\boldsymbol{r}_j$ is the coordinate of atom j in this unit cell and $\boldsymbol{u}(\boldsymbol{R}_{nj})$ is the displacement from this ideal lattice

point. Substituting this expression for the electron density into (1) and changing variables in each term, the scattering amplitude can be written as an infinite sum over the unit cells:

$$A(\boldsymbol{q}) = \sum_{n=1}^{N} F_n(\boldsymbol{q}) \mathrm{e}^{-\mathrm{i}\boldsymbol{q}\cdot\boldsymbol{u}(\boldsymbol{R}_n)} \mathrm{e}^{-\mathrm{i}\boldsymbol{q}\cdot\boldsymbol{R}_n} \tag{2}$$

where

$$F_n(\boldsymbol{q}) = \sum_{j=1}^{S} f_{nj}(\boldsymbol{q}) \mathrm{e}^{-\mathrm{i}\boldsymbol{q}\cdot\boldsymbol{r}_j}$$

is the structure amplitude of the nth cell and

$$f_{nj}(\boldsymbol{q}) = \int \rho_{nj}(\boldsymbol{r}') \mathrm{e}^{-\mathrm{i}\boldsymbol{q}\cdot\boldsymbol{r}'} \, \mathrm{d}\boldsymbol{r}'$$

is the atomic scattering factor of an atom j in the unit cell n. Here we are assuming that all atoms in the unit cell are displaced uniformly: $\boldsymbol{u}(\boldsymbol{R}_{nj}) \equiv \boldsymbol{u}(\boldsymbol{R}_n + \boldsymbol{r}_j) = \boldsymbol{u}(\boldsymbol{R}_n)$. It is important to note here that equation (2) is also valid for the more general case allowing different displacements of atoms in different unit cells but with another definition of structure amplitude $F_n(\boldsymbol{q})$ [18]. In general the structure factor $F_n(\boldsymbol{q})$ is a complex function.

Now we will consider the scattering of x-rays by a crystal with finite size. Introducing the finite dimensions leads to 'spreading' of the δ-type intensity distributions characterizing an infinite crystal. The scattering amplitude $A(\boldsymbol{q})$, equation (2), can now be conveniently calculated by means of the approach originally proposed by von Laue [1], which reduces the sum over the points of the ideal lattice within the volume of the finite crystal to an integral over all space. According to this approach (see also [16, 18]), equation (2) can be equivalently rewritten in the form

$$A(\boldsymbol{q}) = F(\boldsymbol{q}) \int \rho_\infty(\boldsymbol{r}) S(\boldsymbol{r}) \mathrm{e}^{-\mathrm{i}\boldsymbol{q}\cdot\boldsymbol{r}} \, \mathrm{d}\boldsymbol{r} \tag{3}$$

where it is assumed that the structure factors of the different cells are identical ($F_n(\boldsymbol{q}) = F(\boldsymbol{q})$) and integration is carried out over the whole space. In this equation

$$\rho_\infty(\boldsymbol{r}) = \sum_{n=1}^{\infty} \delta(\boldsymbol{r} - \boldsymbol{R}_n)$$

is a periodic function with summation over n carried out over all points of an infinite ideal lattice. In the integral (3), this function is multiplied by a *complex* function

$$S(\boldsymbol{r}) = s(\boldsymbol{r}) \exp(-\mathrm{i}\boldsymbol{q} \cdot \boldsymbol{u}(\boldsymbol{r}))$$

with an amplitude $s(\boldsymbol{r})$ equal to unity inside the volume of the crystal and zero outside (the so-called Ewald function [4]) and the phase $\phi(\boldsymbol{r}) = \boldsymbol{q} \cdot \boldsymbol{u}(\boldsymbol{r})$. What is important to note here is that we do not have any restrictions on the shape of the crystal and deformation field.

From the theory of the Fourier transformations, the integral in (3) can be calculated in the form of a convolution of the Fourier integrals of the factors:

$$A(\boldsymbol{q}) = \frac{F(\boldsymbol{q})}{(2\pi)^3} \int \rho_\infty(\boldsymbol{q}') S(\boldsymbol{q} - \boldsymbol{q}') \, \mathrm{d}\boldsymbol{q}' \tag{4}$$

where $S(\boldsymbol{q}')$ is the Fourier integral of $S(\boldsymbol{r})$:

$$S(\boldsymbol{q}') = \int S(\boldsymbol{r}) \mathrm{e}^{-\mathrm{i}\boldsymbol{q}'\cdot\boldsymbol{r}} \, \mathrm{d}\boldsymbol{r} = \int s(\boldsymbol{r}) \mathrm{e}^{-\mathrm{i}\boldsymbol{q}\cdot\boldsymbol{u}(\boldsymbol{r})} \mathrm{e}^{-\mathrm{i}\boldsymbol{q}'\cdot\boldsymbol{r}} \, \mathrm{d}\boldsymbol{r} \tag{5}$$

and the integration over $\mathrm{d}\boldsymbol{q}'$ and that over $\mathrm{d}\boldsymbol{r}$ are carried out over the whole space. If the particle is unstrained, $\boldsymbol{u}(\boldsymbol{r}) \equiv 0$ and we have for the FT (5)

$$s(\boldsymbol{q}) = \int s(\boldsymbol{r}) \mathrm{e}^{-\mathrm{i}\boldsymbol{q}\cdot\boldsymbol{r}} \, \mathrm{d}\boldsymbol{r}. \tag{6}$$

It can easily be shown that for an ideal crystal lattice the Fourier integral of the function $\rho_\infty(\boldsymbol{r})$ reduces to the sum of δ-functions

$$\rho_\infty(\boldsymbol{q}) = \int \rho_\infty(\boldsymbol{r}) \mathrm{e}^{-\mathrm{i}\boldsymbol{q}\cdot\boldsymbol{r}}\, \mathrm{d}\boldsymbol{r} = [(2\pi)^3/v] \sum_n \delta(\boldsymbol{q} - \boldsymbol{h}_n)$$

where v is the volume of the unit cell, $\boldsymbol{h}_n = 2\pi \boldsymbol{H}_n$, the $\boldsymbol{H}_n$ being the reciprocal-lattice vectors, and the summation is carried out over all the reciprocal-lattice points. Taking all of this into account, we obtain for the amplitude (4)

$$A(\boldsymbol{q}) = \frac{F(\boldsymbol{q})}{v} \sum_n A_n(\boldsymbol{q} - \boldsymbol{h}_n) \tag{7}$$

with $A_n(\boldsymbol{q} - \boldsymbol{h}_n) = S(\boldsymbol{q} - \boldsymbol{h}_n)$. From this expression we can see that the scattering amplitude is directly connected with the FT of the complex 'shape' function $S(\boldsymbol{r})$, and its phase for the fixed reciprocal-lattice point $\boldsymbol{h}$ is a sum of phases of the structure factor $F(\boldsymbol{h})$ and the function $S(\boldsymbol{q})$.

For a crystal of microscopic dimensions, the function $S(\boldsymbol{q})$ has appreciable values only for small $\boldsymbol{q}$, much smaller than the reciprocal-lattice parameters. Thus according to (7) and neglecting the small cross-terms, the intensity of the scattering by crystals of finite dimensions will be determined by a sum over reciprocal-lattice points:

$$I(\boldsymbol{q}) = |A(\boldsymbol{q})|^2 = \frac{|F(\boldsymbol{q})|^2}{v^2} \sum_n |A_n(\boldsymbol{q} - \boldsymbol{h}_n)|^2. \tag{8}$$

In the vicinity of the reciprocal point $\boldsymbol{h}_n = \boldsymbol{h}$, $\boldsymbol{q} \simeq \boldsymbol{h}$ and we have for the intensity distribution

$$I(\boldsymbol{Q}) = \frac{|F(\boldsymbol{h})|^2}{v^2} |A_{\boldsymbol{h}}(\boldsymbol{Q})|^2 \tag{9}$$

where $\boldsymbol{Q} = \boldsymbol{q} - \boldsymbol{h}$ and

$$A_{\boldsymbol{h}}(\boldsymbol{Q}) = \int s(\boldsymbol{r}) \mathrm{e}^{-\mathrm{i}\boldsymbol{h}\cdot\boldsymbol{u}(\boldsymbol{r})} \mathrm{e}^{-\mathrm{i}\boldsymbol{Q}\cdot\boldsymbol{r}}\, \mathrm{d}\boldsymbol{r}. \tag{10}$$

Some general properties of this distribution should be outlined. For any arbitrary form of the crystal, the intensity distribution (8) as a function of $\boldsymbol{q}$ is a periodic function. For the special case of unstrained particles ($\boldsymbol{u}(\boldsymbol{r}) \equiv 0$), the intensity distribution is locally centrosymmetric around *every* $\boldsymbol{h}_n$ and has the same shape for *every* reciprocal-lattice point $\boldsymbol{h}_n$. It takes its maximum value of $|F(\boldsymbol{h}_n)|^2 V^2/v^2$ if the scattering vector is exactly equal to $\boldsymbol{q} = \boldsymbol{h}_n$ and this point is the centre of symmetry of the intensity distribution $I(\boldsymbol{q})$ (since according to (6), $s(-\boldsymbol{q}) = s^*(\boldsymbol{q})$). This reproducibility of the distribution is a characteristic of the broadening effect associated with the finite size of the crystal; effects associated with strain $\boldsymbol{u}(\boldsymbol{r})$ lead to different distributions near different reciprocal-lattice points. The possibilities of mapping this strain field directly from the intensity measurements during coherent illumination of the particles in 1D, 2D and 3D cases are discussed in recent papers [19, 20].

Equation (8) corresponds to the situation where *one* particle is illuminated by a coherent beam. In the case where two or more crystallites are located at some distance apart and are illuminated by the same coherent beam, interference terms will appear in the expression for the intensity (8). An especially interesting intensity distribution can be obtained in the case where a small particle is separated sufficiently from a big one and illuminated by the same coherent beam. This is similar to the principles of Fourier holography, where the object can be found as one term in the autocorrelation [21].

As follows from the previous analysis, the simplest picture of identical repeated distributions with dimensions of the order of the reciprocal dimensions of the crystal arises in unstrained crystals of any arbitrary shape. The detailed 3D shape of this distribution is determined by the Fourier components of the function (10) with $\boldsymbol{u}(\boldsymbol{r}) = 0$ (in this case, $A_{\boldsymbol{h}}(\boldsymbol{Q}) \equiv s(\boldsymbol{Q})$ from equation (6)). Calculations of $s(\boldsymbol{Q})$ for crystals of different shapes, in particular for polyhedra with arbitrary crystallographic boundaries, are given in [1, 2, 22]. The shapes of the intensity patterns detected by a 2D detector (such as a CCD camera) depend also on the Bragg angle and on the departure from the exact Bragg condition (the detector plane is always perpendicular to the $\boldsymbol{k}_f$-vector). If the z-axis in reciprocal space is directed along the $\boldsymbol{k}_f$-vector and the detector itself is exactly at a Bragg point, then we have from (6)–(10) the following distribution of the amplitude:

$$A(Q_x, Q_y) = \frac{F(\boldsymbol{h})}{v} \int s_z(x, y) \mathrm{e}^{-\mathrm{i}Q_x x - \mathrm{i}Q_y y} \, \mathrm{d}x \, \mathrm{d}y \tag{11}$$

where $s_z(x, y) = \int \mathrm{d}z \; s(x, y, z)$. So the inverse FT of the amplitude distribution (11) at the Bragg point gives the projection of the crystal shape on the (x, y) plane. In figure 1, calculations

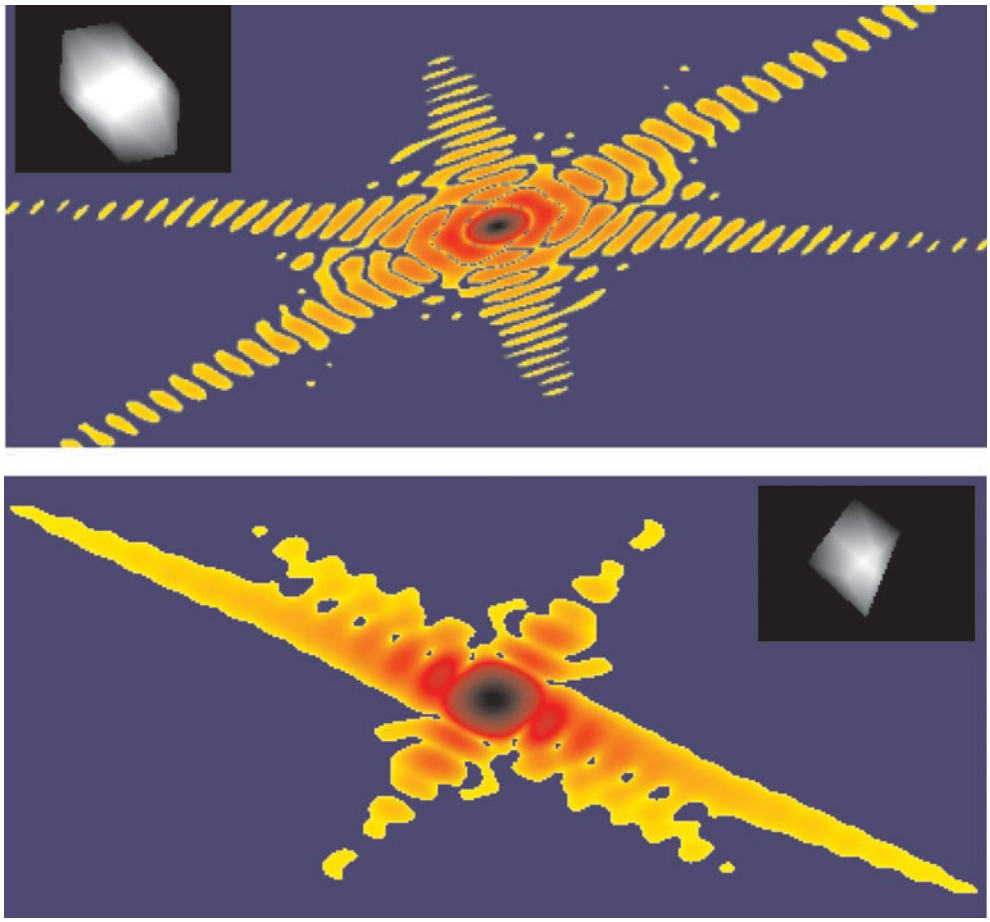

Figure 1. Projection of the different crystal shapes on the plane perpendicular to $\boldsymbol{k}_f$ and the corresponding diffraction pattern calculated at the exact Bragg position.

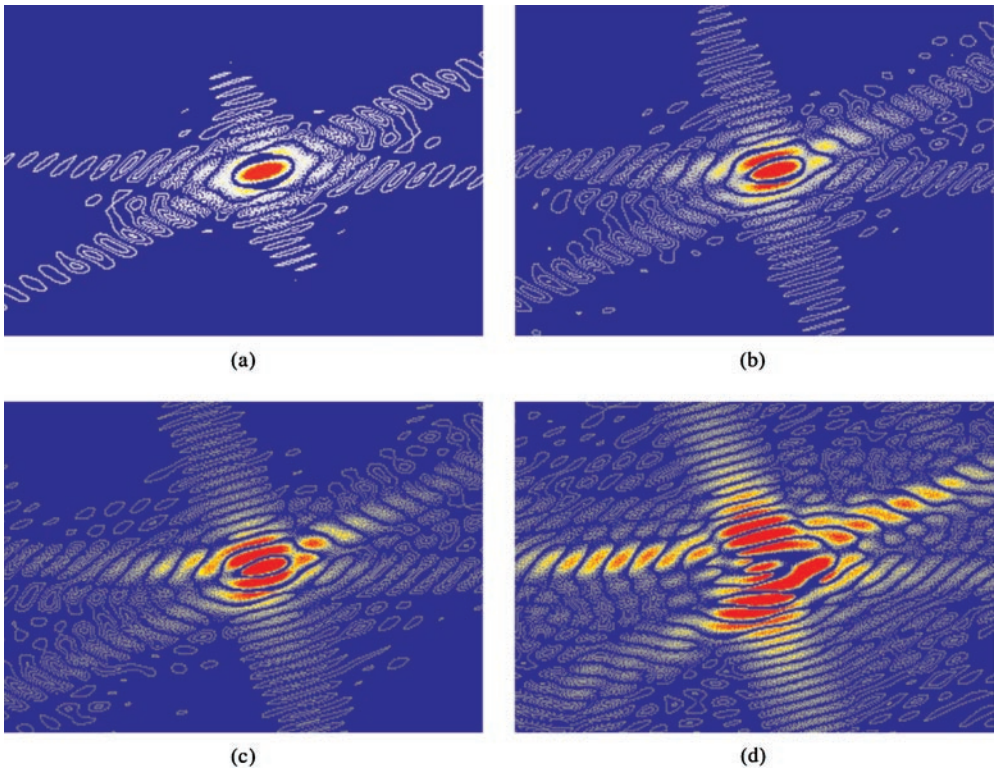

Figure 2. The cross-section of the reciprocal space of the diffraction pattern produced from the crystal shape shown in the insets of figure 1 for different q_z-values: $q_z = 0$, $q_z = 0.357\ q_D$, $q_z = 0.476\ q_D$, $q_z = 1.19\ q_D$. Here q_D corresponds to the fringe spacing: $q_D \sim 2\pi/D$. The intensity in the figure is rescaled for clarity.

of the amplitude (11) for different crystal shapes are presented. Cuts of the reciprocal space for values of Q_z other than $Q_z = 0$ can also be calculated using the 2D FT (11) with the change of the real function $s_z(x, y)$ to a complex-valued function:

$$s_z(x, y, Q_z) = \int \mathrm{d}z\, s(x, y, z) \exp(\mathrm{i}Q_z z).$$

Examples of such calculations for different values of Q_z and one of the crystal shapes from figure 1 are presented in figure 2.

As was proposed by von Laue [1], applying Green's theorem to (6) the volume integral can be transformed to an integral with the integration taken over the external surface of the crystal:

$$s(\boldsymbol{q}) = \frac{\mathrm{i}}{q^2} \int_S (\boldsymbol{q} \cdot \boldsymbol{n}) \mathrm{e}^{-\mathrm{i}\boldsymbol{q}\cdot\boldsymbol{r}}\, \mathrm{d}\sigma \tag{12}$$

where the unit vector $\boldsymbol{n}$ is an outward normal to the crystal surface. The maximum of this distribution for the flat surface is along directions normal to the surface and gives the origin of the crystal truncation rod distribution [23] or asymptotic Bragg diffraction [24] widely studied in diffraction from surfaces. In the case of the crystal with a centre of symmetry and with a pair of identical opposite faces, we have from (12)

$$s(\boldsymbol{q}) = 2\frac{(\boldsymbol{q} \cdot \boldsymbol{n})}{q^2} \int_S \sin(\boldsymbol{q} \cdot \boldsymbol{r})\, \mathrm{d}\sigma. \tag{13}$$

If the distance between faces is equal to D, then for the direction of $\boldsymbol{q}$ perpendicular to the faces, we obtain for this distribution

$$s(q) = \frac{2}{q} S \sin(qD/2). \tag{14}$$

As follows from this result, in the case of two opposite faces and coherent illumination we immediately obtain an *interference* pattern for the intensity distribution rather than the smooth q^{-1}-decrease of amplitude for one surface. The integral width of this intensity distribution in reciprocal space is equal to $\delta q = 2\pi/D$. This leads to a rod-like shape intensity distribution for crystals shaped like a compressed disc. Such behaviour was for example observed in [25], where thin films (with thickness 2000 Å) of the binary alloy Cu_3Au were illuminated by a coherent x-ray beam. Due to its antiphase domain structure the superstructure Bragg diffraction from these films produces a speckle image on the CCD detector. As was demonstrated in [25], these speckles are highly elongated in reciprocal space along the normal to the surface of the Cu_3Au film due to the small thickness of the film. In the case of a flat surface, the same Green's theorem can be applied once more to equation (12), transforming the surface integral to an integral around the boundary of the face S and producing additional fringes for a pair of opposite flat edges.

In conclusion, we can see that any pair of opposite faces and corresponding edges of an unstrained crystal in a coherent beam will produce an interference pattern with the maximum distribution along the normal to the face and perpendicular to the opposite surface edges (see figure 1).

3. Partially coherent radiation

In the previous section the case of totally coherent incident radiation was considered. Now we will assume that the incoming beam is partially coherent. The general properties of partially coherent radiation are discussed in detail in a number of textbooks [26–28]. The comprehensive theory of scattering of a partially coherent *x-ray* wave-field in both Fresnel and Fraunhofer limits was given by Sinha, Tolan and Gibaud [13]. We will reformulate this general results for the special case of scattering of partially coherent x-ray radiation by small crystalline particles. The whole problem will be divided into two parts. In the first part we consider scattering of radiation with an arbitrary state of coherence by a small crystal particle and in the second the special form of the incoherent source with Gaussian distribution of the intensity will be considered.

We will take the incident radiation in the form of a quasimonochromatic wave with only one polarization state of the electric field:

$$E_{in}(\boldsymbol{r}, t) = A_{in}(\boldsymbol{r}, t) \mathrm{e}^{\mathrm{i}\boldsymbol{k}_i \cdot \boldsymbol{r} - \mathrm{i}\bar{\omega} t} \tag{15}$$

where $|\boldsymbol{k}| = 2\pi/\bar{\lambda}$ and $\bar{\lambda}, \bar{\omega}$ are the average wavelength and frequency of the beam. The amplitude $A_{in}(\boldsymbol{r}, t)$ is a slowly varying function with spatial variations much bigger than the wavelength $\bar{\lambda}$ and timescales much larger than $1/\bar{\omega}$. Then, according to the standard Huygens–Fresnel principle [26], in the limits of kinematical scattering, the amplitude of the wave-field $E_{out}(\boldsymbol{v}, t)$, after scattering from the sample to position $\boldsymbol{v}$ on the detector (figure 3(a)), can be written as[2]

$$E_{out}(\boldsymbol{v}, t) = \int \mathrm{d}\boldsymbol{r}\, \rho(\boldsymbol{r}) \frac{A_{in}(\boldsymbol{r}, t - \tau_r)}{l_r} \mathrm{e}^{\mathrm{i}\boldsymbol{k}_i \cdot \boldsymbol{r} - \mathrm{i}\bar{\omega}(t - \tau_r)} \tag{16}$$

[2] In this expression and below, we will omit all inessential integral prefactors.

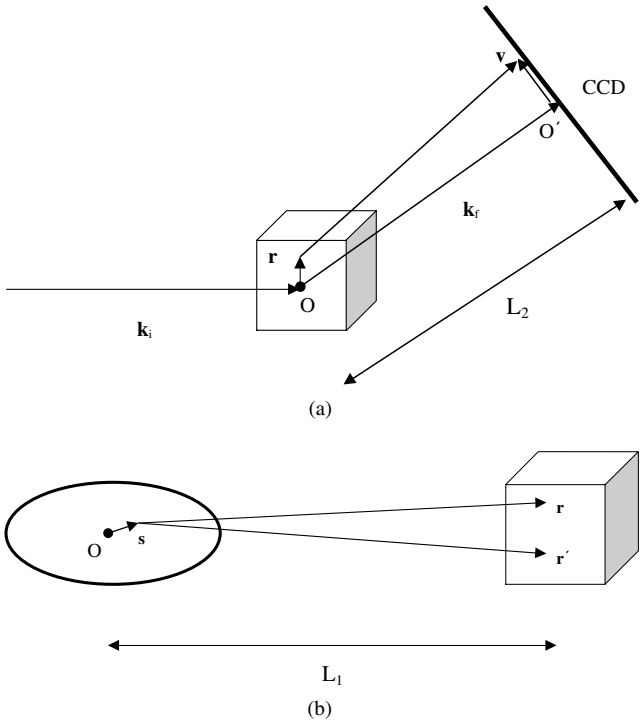

Figure 3. Definition of the notation used for the scattering geometry in the calculation of the scattering of the partial coherent radiation. (a) The x-ray beam is scattered by a small crystal particle and the intensity is measured at a distance L_2 from the sample by a 2D detector (CCD camera). (b) A synchrotron source produces an incoherent beam at the distance L_1 from the sample.

where l_r is the distance between points $\boldsymbol{r}$ and $\boldsymbol{v}$ with the origins at the sample centre and in the detector plane respectively, $\tau_r = l_r/c$ is the time delay for the radiation propagation between the same points and c is the speed of light. In this expression for the scattered wave-field we have neglected absorption in a small sample and set the obliquity factor as $\chi \approx 1$.

We will define the amplitude of scattering $A(\boldsymbol{v}, t)$ in the usual way:

$$E_{out}(\boldsymbol{v}, t) = A(\boldsymbol{v}, t)\left(\mathrm{e}^{\mathrm{i}kL_2}/L_2\right)\mathrm{e}^{-\mathrm{i}\bar{\omega}t}.$$

Then assuming that the distance from the object to the detector $L_2 \gg D$, where D is a typical size of an object, we would have the usual expansion in the limits of the paraxial approximation for the distance l_r between points $\boldsymbol{r}$ and $\boldsymbol{v}$:

$$l_r \simeq L_2 - \boldsymbol{n}_f \cdot \boldsymbol{r} + (\boldsymbol{v} - \boldsymbol{r})^2/(2L_2)$$

where $\boldsymbol{n}_f = \boldsymbol{k}_f/|\boldsymbol{k}_f|$. Here we also assumed that the detector plane is perpendicular to $\boldsymbol{k}_f$. Substituting this expansion into equation (16) we obtain for the scattering amplitude

$$A(\boldsymbol{v}, t) = \int \mathrm{d}\boldsymbol{r}\, \rho(\boldsymbol{r}) A_{in}(\boldsymbol{r}, t - \tau_r) P_{L_2}(\boldsymbol{v} - \boldsymbol{r})\mathrm{e}^{-\mathrm{i}\boldsymbol{q}\cdot\boldsymbol{r}} \tag{17}$$

where $P_{L_2}(\boldsymbol{v} - \boldsymbol{r})$ is the Green's function (or propagator) that describes the propagation of radiation in free space. In the framework of the same theory this function is equal to

$$P_{L_2}(\boldsymbol{v} - \boldsymbol{r}) = \frac{1}{\mathrm{i}\lambda L_2}\mathrm{e}^{\mathrm{i}(k/2L_2)(\boldsymbol{v}-\boldsymbol{r})^2}. \tag{18}$$

We will be interested in the far-field (or Fraunhofer) limit of equation (17), where the condition $kD^2/(2L_2) \ll 1$ is satisfied. For a typical coherent x-ray experiment with radiation energy $E_\gamma \simeq 8$ keV and a detector at a distance $L_2 \simeq 3$ m, this condition limits the size of the particles: $D \ll 10\,\mu$m. In this limit we can neglect the $(k/2L_2)\boldsymbol{r}^2$ term in the exponent (18) and have for the propagator

$$P_{L_2}(\boldsymbol{v}-\boldsymbol{r}) \underset{\lim(kD^2)/L_2\to 0}{\longrightarrow} (1/\mathrm{i}\lambda L_2)\exp\left[\mathrm{i}(k/2L_2)\boldsymbol{v}^2\right]\exp(-\mathrm{i}\boldsymbol{q}_v\cdot\boldsymbol{r})$$

where $\boldsymbol{q}_v = (k/L_2)\boldsymbol{v}$. So, in the far field we obtain for the amplitude (17)

$$A(\boldsymbol{q}',t) = \int \mathrm{d}\boldsymbol{r}\,\rho(\boldsymbol{r})A_{in}(\boldsymbol{r},t-\tau_r)\mathrm{e}^{-\mathrm{i}\boldsymbol{q}'\cdot\boldsymbol{r}} \tag{19}$$

where $\boldsymbol{q}' = \boldsymbol{q}+\boldsymbol{q}_v$. Here we omit the phase term $\exp[\mathrm{i}(k/2L_2)\boldsymbol{v}^2]$ before the integral because it will cancel while calculating intensities at the same point $\boldsymbol{v}$ in the detector plane. We would like to note here that this expression coincides with the coherent amplitude of equation (1) in the limit $A_{in}(\boldsymbol{r},t-\tau_r)\to 1$. Now, we will consider the case where the scattering particle is a crystalline sample with a periodic electron density function and the amplitude $A_{in}(\boldsymbol{r},t-\tau_r)$ is a slowly varying function of the size of the unit cell. Under these conditions, performing the same transformations as in the previous section, we finally obtain

$$A(\boldsymbol{q}',t) = \frac{F(\boldsymbol{q})}{v}\sum_n A_n(\boldsymbol{q}'-\boldsymbol{h}_n,t) \tag{20}$$

where

$$A_n(\boldsymbol{q},t) = \int \mathrm{d}\boldsymbol{r}\,s(\boldsymbol{r})A_{in}(\boldsymbol{r},t-\tau_r)\mathrm{e}^{-\mathrm{i}\boldsymbol{q}\cdot\boldsymbol{r}}. \tag{21}$$

Here, as before, $s(\boldsymbol{r})$ is a shape function of the crystal and for simplicity we are assuming that the crystal is unstrained. However, this result can be generalized also for the case of the strained crystal by adding the exponential factor $\exp[-\mathrm{i}\boldsymbol{q}\cdot\boldsymbol{u}(\boldsymbol{r})]$ to the integral (21).

The intensity of the scattered radiation measured at the position $\boldsymbol{v}$ of the detector near one of the Bragg points $\boldsymbol{h}_n = \boldsymbol{h}$, according to (20), (21), is equal to

$$\begin{aligned} I(\boldsymbol{Q}) &= \langle A(\boldsymbol{Q},t)A^*(\boldsymbol{Q},t)\rangle_T = \frac{|F(\boldsymbol{h})|^2}{v^2}\,|A_h(\boldsymbol{Q},t)|^2 \\ &= \frac{|F(\boldsymbol{h})|^2}{v^2}\int\int \mathrm{d}\boldsymbol{r}\,\mathrm{d}\boldsymbol{r}'\,s(\boldsymbol{r})s(\boldsymbol{r}')\Gamma_{in}(\boldsymbol{r},\boldsymbol{r}',\Delta\tau)\mathrm{e}^{-\mathrm{i}\boldsymbol{Q}\cdot(\boldsymbol{r}-\boldsymbol{r}')} \end{aligned} \tag{22}$$

where $\boldsymbol{Q} = \boldsymbol{q}'-\boldsymbol{h} = \boldsymbol{q}_v+\boldsymbol{q}-\boldsymbol{h}$, $\Delta\tau = (l_r - l_{r'})/c$ is a time delay and

$$\Gamma_{in}(\boldsymbol{r},\boldsymbol{r}',\tau) = \langle A_{in}(\boldsymbol{r},t)A^*_{in}(\boldsymbol{r}',t+\tau)\rangle_T \tag{23}$$

is the mutual coherence function. Averaging in (22) and (23) is carried out for time T much longer than the time of fluctuation of the x-ray field and it is assumed that the incoming radiation is ergodic and stationary. For the case of cross-spectral pure light we can write the mutual coherence function as a product [27, 28]:

$$\Gamma_{in}(\boldsymbol{r},\boldsymbol{r}',\tau) = \sqrt{I(\boldsymbol{r})}\sqrt{I(\boldsymbol{r}')}\gamma_{in}(\boldsymbol{r},\boldsymbol{r}')F(\tau) \tag{24}$$

where $I(\boldsymbol{r}) = \langle|A_{in}(\boldsymbol{r},t)|^2\rangle_T$ and $I(\boldsymbol{r}') = \langle|A_{in}(\boldsymbol{r}',t)|^2\rangle_T$ are the averaged intensities of the incoming radiation at points $\boldsymbol{r}$ and $\boldsymbol{r}'$, $\gamma_{in}(\boldsymbol{r},\boldsymbol{r}')$ is a normalized mutual coherence function or complex degree of coherence and $F(\tau)$ is the time autocorrelation function.

We will make some more simplifying assumptions so as to obtain an explicit form for the mutual coherence function (24). We will assume that the incident radiation is coming from a planar incoherent source with a Gaussian distribution of intensity located at a distance L_1 from

the sample (figure 3). This will be an approximation for the actual 3D electron 'bunch' source from the synchrotron storage ring. We will also consider the distance L_1 to be much larger than both the size of the particle D and an average size of the source S. In the same limit of the paraxial approximation, the complex degree of coherence $\gamma_{in}(\boldsymbol{r}, \boldsymbol{r}')$ can be obtained according to the van Cittert–Zernike theorem [26, 27]:

$$\gamma_{in}(\boldsymbol{r}-\boldsymbol{r}') = \left(\mathrm{e}^{\mathrm{i}\psi}\int \mathrm{d}\boldsymbol{s}\; I(\boldsymbol{s})\mathrm{e}^{-\mathrm{i}(k/L_1)(\boldsymbol{r}-\boldsymbol{r}')\cdot\boldsymbol{s}}\right)\Big/\left(\int \mathrm{d}\boldsymbol{s}\; I(\boldsymbol{s})\right) \tag{25}$$

where the phase factor $\psi = (k/2L_1)(r^2 - r'^2)$, $I(\boldsymbol{s})$ is the intensity distribution of the incoherent source and integration is performed over the whole area of the incoherent source. It is interesting to note here that, for an incoherent source, expression (25) is exact up to second-order terms in s. For the typical CXD experiment on a synchrotron source with distance from source to sample $L_1 \simeq 40$ m and energy $E_\gamma \simeq 8$ keV, the far-field conditions $kD^2/(2L_1) \ll 1$ can be easily satisfied, giving the upper limit for the size of the particle $D \ll 40\,\mu$m. In this far-field limit we can neglect in equation (25) the phase prefactor $\exp[\mathrm{i}\psi]$. For the same model of incoherent source and far-field limit, the intensity of incoming radiation at points $\boldsymbol{r}$ and $\boldsymbol{r}'$ of a sample can be easily calculated as

$$I(\boldsymbol{r}) \simeq I(\boldsymbol{r}') = I_0 = (\lambda/L_1)^2\int I(\boldsymbol{s})\,\mathrm{d}\boldsymbol{s}.$$

It is usual to describe the intensity distribution of the synchrotron source by the Gaussian function

$$I(s_x, s_y) = \frac{I_0}{2\pi\sigma_x\sigma_y}\mathrm{e}^{-\frac{1}{2}\left(s_x^2/\sigma_x^2 - s_y^2/\sigma_y^2\right)} \tag{26}$$

where σ_x and σ_y are the halfwidths of the intensity distribution in the x- and y-directions. Due to the fact that (25) is a FT we also get a Gaussian form for the complex degree of coherence:

$$\gamma_{in}(\boldsymbol{r}_\perp - \boldsymbol{r}'_\perp) = \exp\left(-\frac{(\boldsymbol{r}_\perp - \boldsymbol{r}'_\perp)^2}{2\xi_\perp^2}\right) = \exp\left(-\frac{(x-x')^2}{2\xi_x^2} - \frac{(y-y')^2}{2\xi_y^2}\right). \tag{27}$$

Here $\boldsymbol{r}_\perp$ and $\boldsymbol{r}'_\perp$ are projections of $\boldsymbol{r}$ and $\boldsymbol{r}'$ across the beam propagation direction and $\xi_{x,y} = L_1/(k\sigma_{x,y})$ are usually defined as the two transverse coherence lengths. For typical parameters of the APS source [29, 30], $\sigma_x \simeq 350\,\mu$m, $\sigma_y \simeq 50\,\mu$m, therefore, for the distance $L_1 = 40$ m and radiation $E_\gamma = 8$ keV, we obtain $\xi_x \simeq 3\,\mu$m and $\xi_y \simeq 20\,\mu$m.

We will further assume that the time autocorrelation function $F(\tau)$ in (24) has a pure exponential form:

$$F(\tau) = F_0\exp(-\tau/\tau_\parallel) \tag{28}$$

which is an exact result for a Lorentzian power spectral density of the source [28]. The characteristic time $\tau_\parallel$ of the decay of the time autocorrelation function defines the longitudinal correlation length $\xi_\parallel = c\tau_\parallel$. It can easily be shown [26–28] that the correlation length $\xi_\parallel$ is determined by the bandwidth $(\Delta\lambda/\lambda)$ of the incoming radiation, and for an exponential autocorrelation function $F(\tau)$ it is equal to $\xi_\parallel = (2/\pi)(\lambda^2/\Delta\lambda)$. For a Si(111) double-crystal monochromator with $\Delta\lambda/\lambda \simeq 3\times10^{-4}$ and the wavelength $\lambda \simeq 1.5\,$Å, we get for the longitudinal coherence length $\xi_\parallel \simeq 0.32\,\mu$m.

In the far-field limit we have for the time autocorrelation function $F(\Delta\tau)$

$$F(\Delta\tau) = F(|\boldsymbol{r}_\parallel - \boldsymbol{r}'_\parallel|) = F_0\exp(-|l_r - l_{r'}|/\xi_\parallel) = F_0\exp(-|\boldsymbol{r}_\parallel - \boldsymbol{r}'_\parallel|/\xi_\parallel) \tag{29}$$

where $\boldsymbol{r}_\parallel$ and $\boldsymbol{r}'_\parallel$ are the components of $\boldsymbol{r}$ and $\boldsymbol{r}'$ along the beam direction and we have neglected the small perpendicular contribution.

Substituting expressions (23)–(29) into (22) we now get for the intensity

$$I(\boldsymbol{Q}) = \frac{|F(\boldsymbol{h})|^2}{v^2} \int\int \mathrm{d}\boldsymbol{r}\, \mathrm{d}\boldsymbol{r}'\; s(\boldsymbol{r}) s(\boldsymbol{r}') \gamma_{in}(\boldsymbol{r}_\perp - \boldsymbol{r}'_\perp) F(|\boldsymbol{r}_\parallel - \boldsymbol{r}'_\parallel|) \mathrm{e}^{-\mathrm{i}\boldsymbol{Q}\cdot(\boldsymbol{r}-\boldsymbol{r}')} \tag{30}$$

where the complex degree of coherence $\gamma_{in}(\boldsymbol{r}_\perp - \boldsymbol{r}'_\perp)$ is defined by (27) and the autocorrelation function $F(|\boldsymbol{r}_\parallel - \boldsymbol{r}'_\parallel|)$ by (29). This expression can be further simplified by changing variables:

$$I(\boldsymbol{Q}) = \frac{|F(\boldsymbol{h})|^2}{v^2} \int \mathrm{d}\boldsymbol{r}\; \varphi_{11}(\boldsymbol{r}) \gamma_{in}(\boldsymbol{r}_\perp) F(|\boldsymbol{r}_\parallel|) \mathrm{e}^{-\mathrm{i}\boldsymbol{Q}\cdot\boldsymbol{r}} \tag{31}$$

where

$$\varphi_{11}(\boldsymbol{r}) = \int \mathrm{d}\boldsymbol{r}'\; s(\boldsymbol{r}') s(\boldsymbol{r}' + \boldsymbol{r})$$

is the autocorrelation function of the shape function $s(\boldsymbol{r})$.

In the coherent limit, the transverse and longitudinal coherence lengths $\xi_\perp, \xi_\parallel$ become infinite and that simultaneously leads to the limits for the normalized complex degree of coherence $\gamma_{in}(\boldsymbol{r}_\perp) \to 1$ and the autocorrelation function $F(|\boldsymbol{r}_\parallel|) \to 1$. In this case we get for the intensity of the coherently scattered radiation

$$I_{coh}(\boldsymbol{Q}) = \frac{|F(\boldsymbol{h})|^2}{v^2} \int \mathrm{d}\boldsymbol{r}\; \varphi_{11}(\boldsymbol{r}) \mathrm{e}^{-\mathrm{i}\boldsymbol{Q}\cdot\boldsymbol{r}} = |A(\boldsymbol{Q})|^2 \tag{32}$$

where

$$A(\boldsymbol{Q}) = (F(\boldsymbol{h})/v) \int \mathrm{d}\boldsymbol{r}\; s(\boldsymbol{r}) \mathrm{e}^{-\mathrm{i}\boldsymbol{Q}\cdot\boldsymbol{r}}$$

is a kinematically scattered amplitude from the crystal with shape function $s(\boldsymbol{r})$. This result completely coincides with the coherent limit of equations (9), (10) discussed above.

Using the properties of the Fourier transform, the intensity $I(\boldsymbol{Q})$ in equation (31) can be written in the form of a convolution of two functions:

$$I(\boldsymbol{Q}) = \frac{1}{(2\pi)^3} \int \mathrm{d}\boldsymbol{Q}'\; I_{coh}(\boldsymbol{Q}') \widetilde{\Gamma}(\boldsymbol{Q} - \boldsymbol{Q}') \tag{33}$$

where $I_{coh}(\boldsymbol{Q})$ is the intensity of coherently scattered radiation (32) and $\widetilde{\Gamma}(\boldsymbol{Q})$ is the Fourier transform

$$\widetilde{\Gamma}(\boldsymbol{Q}) = \int \mathrm{d}\boldsymbol{r}\; \gamma_{in}(\boldsymbol{r}_\perp) F(|\boldsymbol{r}_\parallel|) \mathrm{e}^{-\mathrm{i}\boldsymbol{Q}\cdot\boldsymbol{r}}. \tag{34}$$

Now we will consider the same choice of orthogonal coordinates with the $\boldsymbol{z}$-axis along the diffracted beam propagation direction and the $\boldsymbol{x}$-, $\boldsymbol{y}$-axes perpendicular to this direction as in the previous section. In this coordinate system, for the exact Bragg position ($\boldsymbol{q} = \boldsymbol{h}$ and $\boldsymbol{Q} = \boldsymbol{q}_v$) we can write the intensity distribution (31) in the detector plane as

$$I(\boldsymbol{q}_v) = \frac{|F(\boldsymbol{h})|^2}{v^2} \int \mathrm{d}\boldsymbol{x}\; \varphi^z_{11}(\boldsymbol{x}) \gamma_{in}(\boldsymbol{x}) \mathrm{e}^{-\mathrm{i}\boldsymbol{q}_v\cdot\boldsymbol{x}} \tag{35}$$

where $\boldsymbol{x}$ is a 2D vector $\boldsymbol{x} = (x, y)$ and

$$\varphi^z_{11}(\boldsymbol{x}) = \int \mathrm{d}z\; \varphi_{11}(\boldsymbol{r}) \exp(-|z|/\xi_\parallel).$$

It is interesting to note that the intensity distribution (35) can also be calculated as a convolution of the FT of $\varphi^z_{11}(\boldsymbol{q})$ and $\gamma_{in}(\boldsymbol{q})$ (see equation (4)). For the case of large longitudinal length $\xi_\parallel \gg D$, the function $\varphi^z_{11}(\boldsymbol{x})$ gives just the projection of the 3D autocorrelation function on

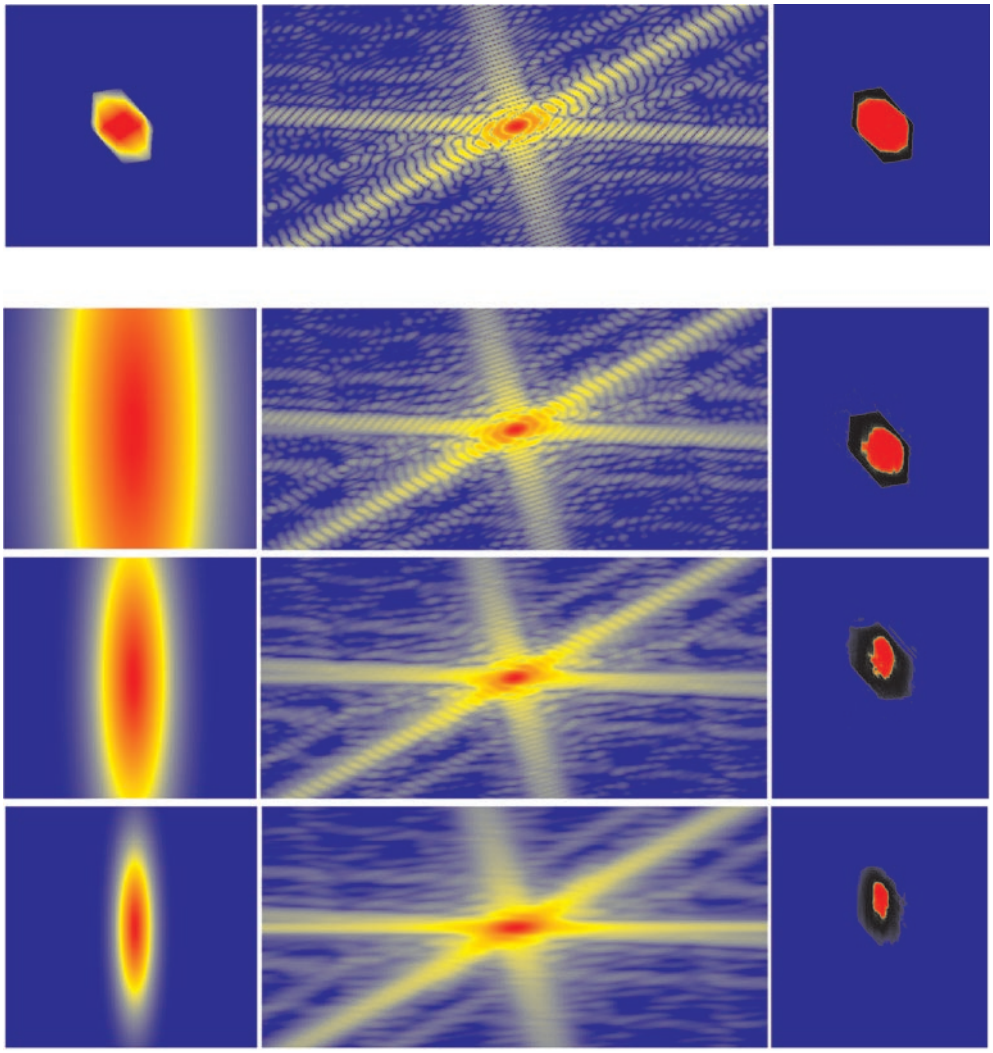

Figure 4. The complex degree of coherence $\gamma_{in}(x, y)$ (left column) used for calculations of diffraction intensity patterns (central column). Reconstructed real-space images are shown in the right column. For comparison, in the top row we show the case of coherent illumination with the coherence lengths $\xi_x, \xi_y = \infty$. The values of the coherence lengths in the other rows are, from the top down: $\xi_x = 91$ pixels, $\xi_y = 367$ pixels; $\xi_x = 45$ pixels, $\xi_y = 183$ pixels; $\xi_x = 22$ pixels, $\xi_y = 91$ pixels.

the plane $\boldsymbol{x}$. Smaller values of $\xi_\parallel \leqslant D$ reduce the real-space volume of the scattering object along the propagating beams that contribute coherently in the diffraction pattern.

In figure 4 we present calculations of 2D diffraction patterns obtained from equation (35) for the crystal shape of figure 1 with different values of the transverse coherence lengths ξ_x, ξ_y. For simplicity we have assumed here that the longitudinal coherence length is big enough, $\xi_\parallel \gg D$, and it will not be considered in our further study. It is readily seen from this figure that decreasing the values of the parameters ξ_x, ξ_y leads to a decrease in the contrast of the diffraction pattern. In the next section we will see how this will affect the reconstructed image of the crystal.

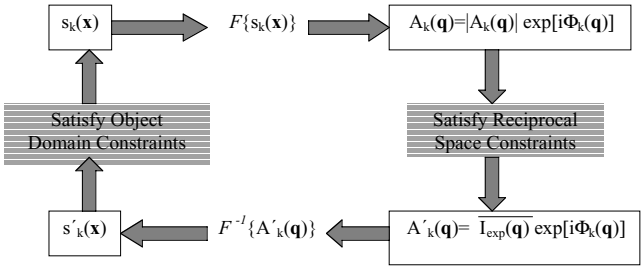

Figure 5. A sketch of iteration procedure used in the reconstruction of the diffraction patterns.

4. Reconstruction of the shape of small crystal objects

Inverse problems arise frequently in physics, and are fundamentally important for optics and crystallography. The magnitude of the FT of some function (in general, complex valued) is measurable, but its phase is not. Various iterative algorithms [6, 7, 10–12, 31] have been applied to solve this problem. Most of them are based on the idea of the Gerchberg–Saxton (GS) algorithm [6] that was originally proposed to solve the problem of retrieving the phase from intensity measurements made in two domains: in real (object) space and reciprocal (experimental data) space. The generalized version of the GS algorithm—the so-called error-reduction (ER) algorithm proposed by Fienup [7]—can be applied to a more general problem, in which partial constraints (in the form of measured data or information known *a priori*), apply in each of the two domains. One simply transforms back and forth between the two domains, satisfying the constraints in one before returning to the other (see figure 5).

For the most general problem the ER algorithm consists of the following four steps (figure 5). In the first step some estimate for an object $s_k(\boldsymbol{x})$ is Fourier transformed:

$$A_k(\boldsymbol{q}) = |A_k(\boldsymbol{q})|\mathrm{e}^{\mathrm{i}\Phi_k(\boldsymbol{q})} = \mathcal{F}[s_k(\boldsymbol{x})].$$

Here $\boldsymbol{x} = (x, y)$ and $\boldsymbol{q} = (q_x, q_y)$ are 2D vectors. Then changes are made in $A_k(\boldsymbol{q})$, to satisfy the reciprocal-space domain constraints to form $A'_k(\boldsymbol{q})$. For the problem of one intensity measurement in reciprocal space, this reduces to the replacement of the modulus of the resulting computed FT by the measured Fourier modulus

$$A'_k(\boldsymbol{q}) = \sqrt{I_{exp}(\boldsymbol{q})}\mathrm{e}^{\mathrm{i}\Phi_k(\boldsymbol{q})}.$$

In the next step, the inverse FT of $A'_k(\boldsymbol{q})$ is calculated:

$$s'_k(\boldsymbol{x}) = |s'_k(\boldsymbol{x})|\mathrm{e}^{\mathrm{i}\theta'_k(\boldsymbol{x})} = \mathcal{F}^{-1}[A'_k(\boldsymbol{q})].$$

Then the minimum changes are made in the resulting computed image $s'_k(\boldsymbol{x})$ to satisfy the object-domain constraints to form $s_{k+1}(\boldsymbol{x})$, a new estimate for the object. In our case the fourth and final step can be formulated as

$$s_{k+1}(\boldsymbol{x}) = \begin{cases} s'_k(\boldsymbol{x}) & \boldsymbol{x} \in S \\ 0 & \boldsymbol{x} \notin S \end{cases} \tag{36}$$

where the support region S is defined as the region in which $s'_k(\boldsymbol{x})$ conforms with the prior knowledge (or estimate) of the size of the object.

To avoid the stagnation problems characteristic of the ER algorithm, it was proposed [7, 10] that the fourth step be modified in such a way that, when the constraint conditions in the real-space domain are not satisfied, the output is pushed in the direction towards satisfying

these conditions. This is called the hybrid input–output (HIO) algorithm. The fourth step now looks as follows:

$$s_{k+1}(\boldsymbol{x}) = \begin{cases} s'_k(\boldsymbol{x}) & |c_k(\boldsymbol{x}) - s'_k(\boldsymbol{x})| < \varepsilon \\ s_k(\boldsymbol{x}) + \beta[c_k(\boldsymbol{x}) - s'_k(\boldsymbol{x})] & |c_k - s'_k(\boldsymbol{x})| > \varepsilon \end{cases} \tag{37}$$

where the parameter β can take values in the range $0 \leqslant \beta \leqslant 1$ and ε is a parameter which allows a small tolerance around the exact constraint. In our tests we found the best values of the parameters β and ε for convergence and fidelity to be $\beta = 0.8$–0.9 and $\varepsilon = 0.01$; these are in good agreement with the previous tests of the algorithm [7, 10]. In the same tests of the iterative algorithms, it was reported that the best strategy for achieving convergence to the desired solution while fitting is to switch between ER and HIO algorithms.

We have gained some experience in applying these methods for reconstruction of the crystal shape $s(\boldsymbol{r})$. We consider that the 2D detector cuts the 3D intensity distribution in reciprocal space perpendicular to the scattered vector $\boldsymbol{k}_f$ exactly through the Bragg position. According to (11) this 2D intensity distribution in the case of coherent illumination is directly connected by the FT with the *projection* of the crystal shape on the plane perpendicular to $\boldsymbol{k}_f$.

The test crystal, shown in figure 1, was taken to have the form of a polyhedron with eight 111 facets and two additional 100 and $\bar{1}00$ facets. The origin was taken as the centre of the symmetry of the crystal. The distance from the origin to the 111 facets was equal to 15 pixels and that to the 100 facets was 20 pixels. This crystal shape was then rotated by 40° around the x-axis and -70° around the y-axis and projected on the (x, y) plane as shown in figure 1. There is uniform density in the middle of the projection and fast changes at the borders. The FFT of this projection shape was calculated with $N_x = 400$ and $N_y = 700$ pixels to produce the diffraction pattern shown in figure 1. This is a typical size for the FFTs used for the diffraction images measured by CCDs in CXD experiments [5].

This diffraction pattern was inverted into a real image by applying the iteration procedure described before. For the problem of reconstruction of the particle projection shape, it is natural to adopt the following constraint conditions for both ER and HIO algorithms: $s'_k(x)$ is real and positive and it lies in the estimated object size S_{object}:

$$c_k(\boldsymbol{x}) = \begin{cases} c'_k = |s'_k(\boldsymbol{x})| \cos\theta'_k \text{ and } c''_k = 0 & \text{if } \boldsymbol{x} \in S_{object} \text{ and } |s'_k(\boldsymbol{x})| \cos\theta'_k > 0 \\ c'_k = 0 \text{ and } c''_k = 0 & \text{if } \boldsymbol{x} \notin S_{object} \text{ or } |s'_k(\boldsymbol{x})| \cos\theta'_k < 0. \end{cases} \tag{38}$$

Schematically, this constraint is shown on the complex c_k-plane in figure 6. A good estimate of the size of the particle in the case of coherent illumination can be obtained from the fringe spacing of the diffraction pattern according to (14). The support region was taken in the form of a rectangular box with lateral size 100×100 pixels which is larger than the size of the particle. The estimated area of the object (support region) S_{object} was compared with the area of the whole image (FFT region) S_{image} to give the oversampling ratio $\sigma = S_{image}/S_{object} = 28$. In this specific case we can easily satisfy the oversampling condition [11] $\sigma \geqslant 2$, which is important for the convergence of the iterative algorithm.

In a typical fitting, we started by generating a real-space complex-valued image $s_0(\boldsymbol{x})$ with amplitude $|s_0(\boldsymbol{x})|$ equal to the support region and random phases $\theta_0(x)$. Then we applied the ER algorithm for 100 cycles alternating with the HIO algorithm for several tens of iterations. This procedure of switching between the HIO and ER cycles was repeated several times. Then calculations were repeated with another set of random phases, and after a number (10–15) of fits, the results were sorted according to increasing value of the residuals, and the best results

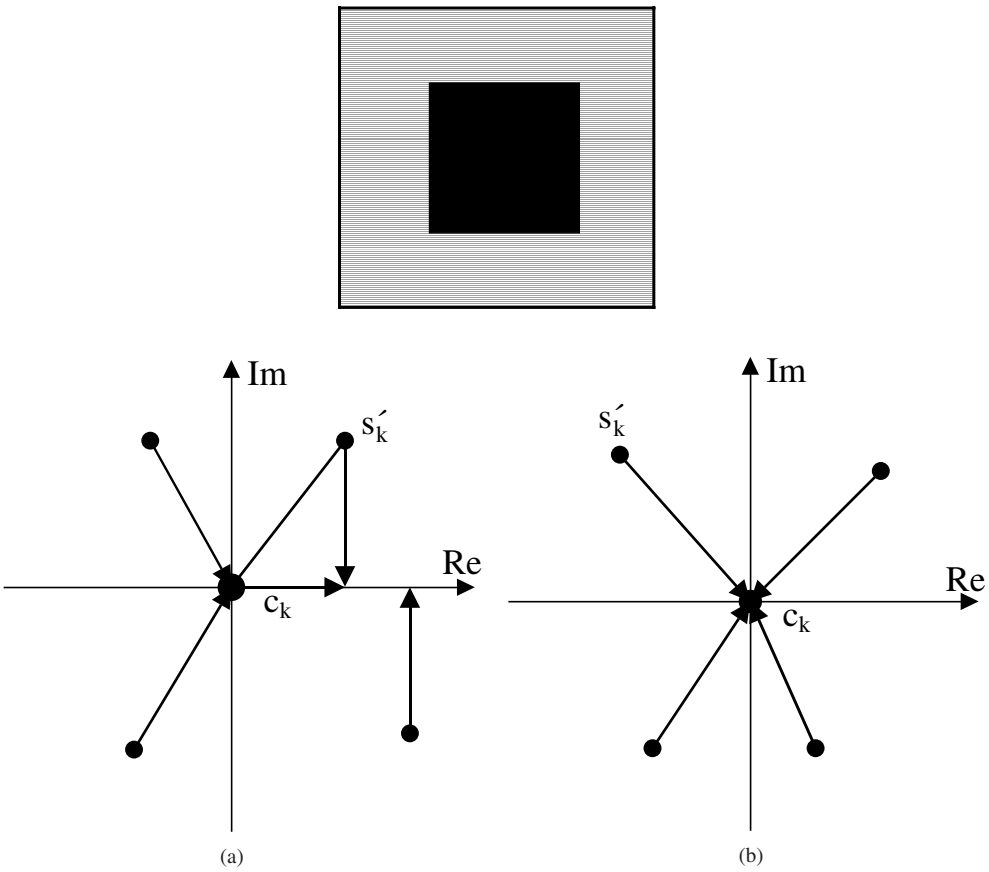

Figure 6. A schematic view of the constraint used in the reconstruction algorithm on the complex space. The left-hand figure corresponds to the situation where the calculation is made within the estimated object size area (the small black box in the middle). The right-hand figure corresponds to the calculation outside this area (the grey area inside the big box).

kept. The error metric in the reciprocal domain was used to monitor the convergence of the algorithm to the solution:

$$E_{A_k} = \left(\sum_{q_x,q_y} \left[|A_k(q_x, q_y)| - \sqrt{I_{exp}(q_x, q_y)} \right]^2 \right) \Big/ \left(\sum_{q_x,q_y} I_{exp}(q_x, q_y) \right). \tag{39}$$

The typical behaviour of the error metric E_{A_k} in the calculations is shown in figure 7(a).

We have found that convergence of the iteration procedure for the most successful fits was already happening after 150 to 200 cycles with the drop of E_{A_k} to 1×10^{-30}. After 200 to 250 iterations we often obtain four or five totally converged images from ten attempts with different starting random phases. It is interesting to note that when a solution was found (usually in the HIO mode), it was maintained in the further cycles of the algorithm; however, switching to the ER mode would result in jumping of the error metric values E_{A_k} up to 1×10^{-7}.

As is clear from our previous discussion, the main assumption of the iterative approach described is that two domains (image and intensity) are *directly* connected by the FT. However, in the real experimental situation it is difficult to calculate or measure with high accuracy the coherency properties of the incoming x-ray beam. In this situation it is desirable to understand

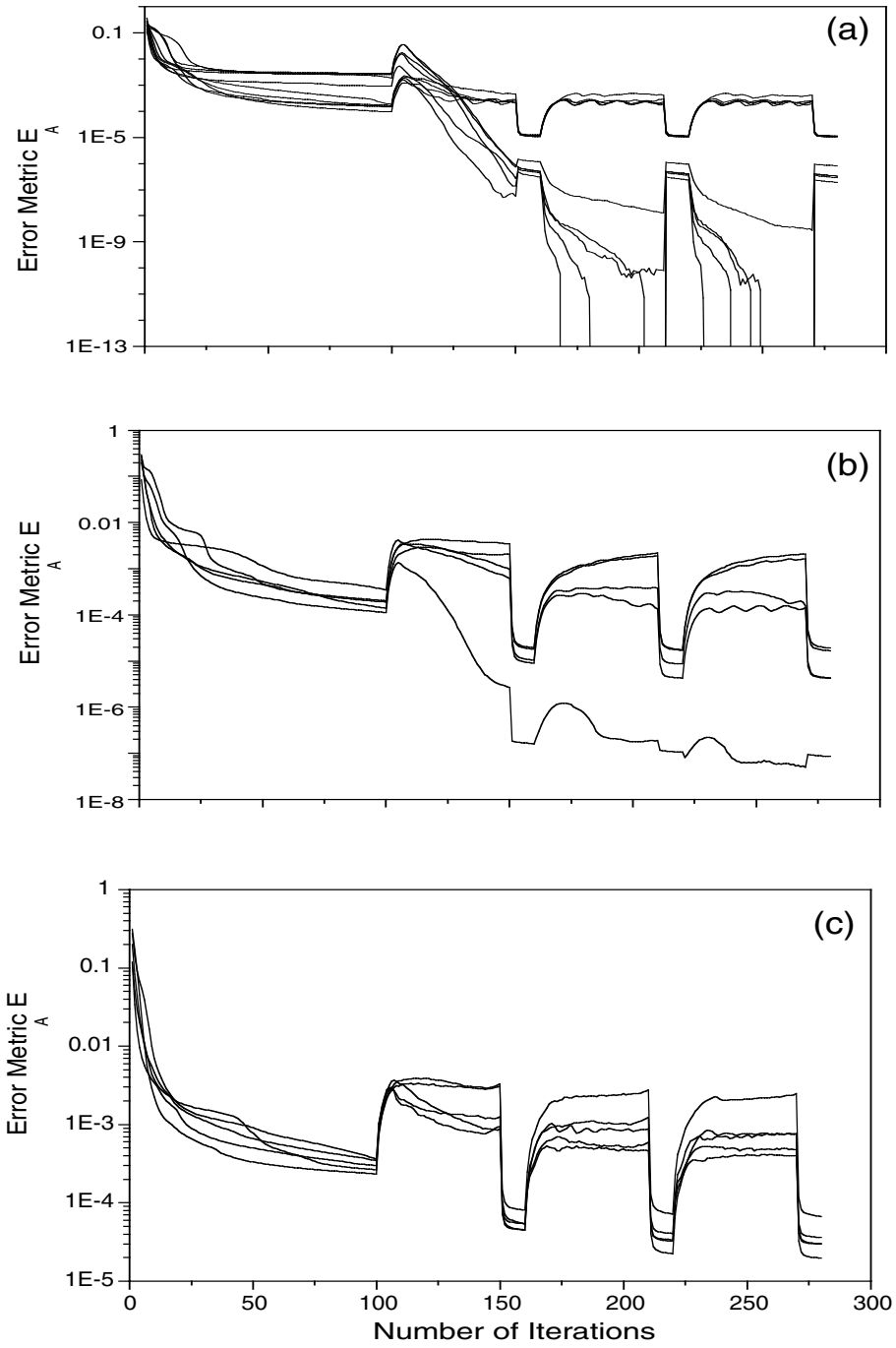

Figure 7. The behaviour of the error metric E_A as a function of the number of iterations. (a) Reconstruction from a pure coherent diffraction image and a small crystal shape. (b) The same case as in (a) but with a twice bigger crystal shape. (c)Reconstruction from a partial coherent diffraction image and a big crystal shape.

Table 1. Results of reconstructions for big particle shapes. Here $\xi_{x,y}$ are the values of the transverse correlation length in pixels, $E_{A\,\mathrm{min}}$ is the best value of the error metric (39), ΔE_A is the difference in this error metric between the best three fits, $\Sigma_{x,y}$(BG) and $\Sigma_{x,y}$(BS) are the sizes of the background and the bright central spot in pixels.

ξ_x	ξ_y	$E_{A\,\mathrm{min}}$	$\Delta E_A/E_{A\,\mathrm{min}}$	Σ_x(BG)	Σ_y(BG)	Σ_x(BS)	Σ_y(BS)
∞	∞	—	—	107.5	127.5	90	92.5
91	367	2.12×10^{-5}	0.11	107.5	127.5	72.5	75
45	183	3.71×10^{-5}	0.25	112.5	127.5	42.5	72.5
22	91	1.98×10^{-5}	0.535	75	125	25	60
11	45	3.9×10^{-6}	0.72	45	115	15	42.5

what the effect of partial coherence on the reconstructed shape of the images would be if no special corrections to compensate for these effects were applied to the diffraction patterns.

To test the effects of partial coherence on the reconstructed shape of the 2D objects, we have used the simulated diffraction patterns from figure 4. Each intensity pattern was calculated according to the theory presented in the previous section with progressively lower values of the transverse coherence ξ_x, ξ_y. These intensity distributions were used to reconstruct the sample shape, applying the iterative algorithms described above.

The results of these tests, shown in figure 4, led to the following observations. First, for the same number of cycles as in the previous tests the error metric E_{A_k} never dropped below the value of 5×10^{-6}. The value of E_{A_k} was becoming even higher, 2×10^{-5}, for lower values of the coherence length. Typical behaviour of E_{A_k} is shown in figure 7(c). Another observation was that for different fits with different choices of random phases, the variation of the error metric E_{A_k} at the end of each fit was bigger than in the case of a purely coherent diffraction pattern. Unlike in the coherent case, the error metric dropped mainly during ER and not HIO cycles. The last observation is the most interesting. For big coherence lengths $\xi_{x,y} \gg D$, the reconstructed object has a uniform distribution of intensity corresponding to the initial projection of the crystal shape. However, when $\xi_{x,y} \sim D$, the maximum intensity region was becoming smaller as well. In the limit of $\xi_{x,y} \ll D$, the densest region had narrowed to a single 'hot' spot. The hot spot in the reconstructed image became narrower as the assumed coherence length $\xi_{x,y}$ was reduced and the error metric became progressively worse. It is not known why the hot spot was shifted from the centre of the real-space image. The same behaviour was observed recently [5] in the reconstruction of experimentally measured CXD patterns for Au particles.

Tables 1 and 2 summarize the results. The reconstructed images have been characterized as a broad background feature (BG), roughly the size of the original object, below a narrower bright spot (BS). In the first two columns of these tables the values of the transverse coherence lengths ξ_x, ξ_y are given in pixels. In the next column the quantity $\Delta E_A/E_A$, where E_A is the best error metric (39) obtained in the reconstruction and ΔE_A is the difference in this error metric between the best three fits, is given. In the next two columns the sizes of the background ($\Sigma_{x,y}$(BG)) and of the bright central spot ($\Sigma_{x,y}$(BS)) in pixels are reported. It is clearly seen from these tables that as soon as the values of the coherence lengths ξ_x, ξ_y start becoming smaller, the size of the bright spot in the centre also starts shrinking—it is in fact of the order of the coherence lengths. At the same time, the background level shows more stability with the reduction of the coherence length.

The appearance of the hot spot can be understood in the following qualitative way. The partial coherence enters equation (33) in the form of a convolution between the ideal intensity

Table 2. Results of reconstructions for small particle shapes.

ξ_x	ξ_y	$E_{A\min}$	$\Delta E_A/E_{A\min}$	Σ_x(BG)	Σ_y(BG)	Σ_x(BS)	Σ_y(BS)
∞	∞	—	—	52.5	62.5	45	45
91	367	3.48×10^{-6}	2.85	52.5	62.5	40	40
45	183	2.79×10^{-5}	0.99	52.5	62.5	35	35
22	91	4.31×10^{-5}	0.18	52.5	62.5	22.5	27.5
11	45	1.72×10^{-5}	1.05	42.5	60	15	30

distribution $I_{coh}(\boldsymbol{Q})$ (perfectly coherent) due to the shape of the object and the Fourier transform of the mutual coherence function $\widetilde{\Gamma}(\boldsymbol{Q})$, which can be assumed to be Gaussian. A compact object, such as a small crystal, will in general have an intensity function with sinusoidal fringes (14). When the fringes are convolved with a Gaussian their amplitude becomes reduced systematically and a smooth broad background appears underneath; this is just the same as the optical diffraction case [26].

In real space, the image of the object becomes multiplied by the complex degree of coherence as seen in equation (31). There are reasons for expecting this complex degree of coherence to have several components arising from optical elements in the experimental set-up. These will therefore be imaged along with the object under investigation. In the limit of small correlation lengths $\xi_{x,y} \ll D$ in the expression for the scattered intensity $I(\boldsymbol{q}_v)$, equation (35), we can take the autocorrelation function $\varphi^z_{11}(\boldsymbol{x})$ out of the integral, obtaining

$$I(\boldsymbol{q}_v) \sim \varphi^z_{11}(0) \int \mathrm{d}\boldsymbol{x}\, \gamma_{in}(\boldsymbol{x}) \mathrm{e}^{-\mathrm{i}\boldsymbol{q}_v \cdot \boldsymbol{x}}.$$

It is clear that inversion of this expression just gives the complex degree of coherence $\gamma_{in}(\boldsymbol{x})$ with the typical size of the area with the maximum intensity $\xi_x \times \xi_y$. It was just this effect that was observed in our test calculations (see tables 1 and 2).

In this paper we have discussed coherent x-ray diffraction for strained crystals under conditions of purely coherent illumination. We have shown how this picture needs to be modified in the case of partially coherent incoming radiation. Different iterative algorithms for reconstruction of this intensity distribution to real-space images were discussed. We have demonstrated and suggested how partial coherence can produce a 'hot' spot on the reconstructed image of a nanocrystal.

Acknowledgments

The authors acknowledge the help of G Williams in the calculation of the diffraction patterns for different crystal shapes and J Pitney for helping develop the computer code. The work was supported by NSF under grant DMR 98-76610.

References

[1] von Laue M 1936 *Ann. Phys. Lpz.* **26** 55
[2] Patterson A L 1939 *Phys. Rev.* **56** 972
[3] Patterson A L 1939 *Phys. Rev.* **56** 978
[4] Ewald P P 1940 *Proc. Phys. Soc.* **52** 167
[5] Robinson I K, Vartanyants I A, Williams G J, Pfeifer M A and Pitney J A 2001 *Phys. Rev. Lett.* at press
[6] Gerchberg R W and Saxton W O 1972 *Optik* **35** 237
[7] Fienup J R 1982 *Appl. Opt.* **21** 2758

[8] Vartanyants I A, Pitney J A, Libbert J L and Robinson I K 1997 *Phys. Rev.* B **55** 13193
[9] Robinson I K, Libbert J L, Vartanyants I A, Pitney J A, Smilgies D M, Abernathy D L and Grübel G 1997 *Phys. Rev.* B **60** 9965
[10] Millane R P and Stroud W J 1997 *J. Opt. Soc. Am.* A **14** 568
[11] Miao J, Sayre D and Chapman H N 1998 *J. Opt. Soc. Am.* A **15** 1662
[12] Miao J, Charalambous P, Kirz J and Sayre D 1999 *Nature* **400** 342
[13] Sinha S K, Tolan M and Gibaud A 1998 *Phys. Rev.* B **57** 2740
[14] Kohn V, Snigireva I and Snigirev A 2000 *Phys. Rev. Lett.* **85** 2745
[15] Lin B, Schlossman M L, Meron M, Williams S M, Huang Z and Viccaro P J 1998 *Phys. Rev.* B **58** 8025
[16] James R W 1982 *The Optical Principles of the Diffraction of X-rays* (Woodbridge, CT: Ox-Bow)
[17] Warren B E 1990 *X-ray Diffraction* (New York: Dover)
[18] Krivoglaz M A 1969 *Theory of X-ray and Thermal-Neutron Scattering by Real Crystals* (New York: Plenum)
[19] Vartanyants I A, Ern C, Donner W, Dosch H and Caliebe W 2000 *Appl. Phys. Lett.* **77** 3929
[20] Robinson I K and Vartanyants I A 2001 *Appl. Surf. Sci.* at press
[21] Leith E N and Upatnieks J *J. Opt. Soc. Am.* **52** 1123
[22] Elistratov A M 1962 *Kristallographiya* **7** 199
[23] Robinson I K 1986 *Phys. Rev.* B **33** 3830
[24] Afanasev A M *et al* 1985 *Acta Crystallogr.* **A41** 227
[25] Pitney J A, Robinson I K, Vartanyants I A, Appleton R and Flynn C P 2000 *Phys. Rev.* B **62** 13084
[26] Born M and Wolf E 1999 *Principles of Optics* 7th edn (Cambridge: Cambridge University Press)
[27] Mandel L and Wolf E 1995 *Optical Coherence and Quantum Optics* (Cambridge: Cambridge University Press)
[28] Goodman J W 1985 *Statistical Optics* (New York: Wiley)
[29] Dejus R J, Lai B, Moog E R and Gluskin E 1994 *Argonne National Laboratory Technical Bulletin* ANL/APS/TB-17
[30] Bizek H M 1996 *Argonne National Laboratory Technical Bulletin* ANL/APS/TB-26
[31] Fienup J R and Wackerman C C 1986 *J. Opt. Soc. Am.* A **3** 1897
[32] Fienup J R, Crimmins T R and Holsztynski W 1982 *J. Opt. Soc. Am.* **72** 610